NUMERICAL SIMULATION OF INERTIAL ENTRAINMENT PHENOMENON

A thesis submitted in partial fulfillment of the requirements for the degree

of

Bachelor of Technology

in

Mechanical Engineering

by

Jatin Kumar Patro (Roll No. 111ME0334)

under the guidance of

Dr. Suman Ghosh

Department of Mechanical Engineering
National Institute of Technology Rourkela

June, 2015

CERTIFICATE

*This is to certify that the thesis entitled "**Numerical Simulation of Inertial Entrainment Phenomenon**", submitted by **Jatin Kumar Patro (Roll Number: 111ME0334)** to National Institute of Technology, Rourkela, is a record of bona fide research work under my supervision, to the best of my knowledge in partial fulfilment of the requirements for the degree of **Bachelor of Technology** in the Department of Mechanical Engineering, National Institute of Technology Rourkela.*

Place: Rourkela
Date:

Dr. Suman Ghosh
Assistant Professor
Department of Mechanical Engineering
National Institute of Technology, Rourkela

DECLARATION

I certify that

a) The work contained in the thesis is original and has been done by myself under the general supervision of my supervisor.

b) The work has not been submitted to any other Institute for any degree or diploma.

c) I have followed the guidelines provided by the Institute in writing the thesis.

d) I have conformed to the norms and guidelines given in the Ethical Code of Conduct of the Institute.

e) Whenever I have used materials (data, theoretical analysis, and text) from other sources, I have given due credit to them by citing them in the text of the thesis and giving their details in the references.

f) Whenever I have quoted written materials from other sources, I have put them under quotation marks and given due credit to the sources by citing them and giving required details in the references.

Place: Rourkela
Date:

Signature of the Student
Jatin Kumar Patro (111me0334)

ACKNOWLEDGMENT

I would like to express my gratitude to my Supervisor Dr. Suman Ghosh for his support and guidance during this project. I am greatly thankful to him for giving me this opportunity to work with him and for believing in me throughout course of completion of this project. Like a true mentor, he has supported and guided us in every step and also helped us to tackle every problem faced during the project. I find myself grateful to have him as my mentor.

I would also like to thank Dr. S.S. Mohapatra, H.O.D, Department of Mechanical Engineering, N.I.T Rourkela, for allowing us to work in lab for extended duration and granting access to departmental facilities. I would also like to thank the staff of Mechanical Department for providing me necessary amenities to finish this project.

Last but not the least; I would like to express my deep gratitude to God and my parents for their blessings without which this task could never have been accomplished.

Place: Rourkela, **Jatin Kumar Patro**

Date: **Roll Number: 111ME0334**

CONTENTS

LIST OF FIGURES

LIST OF EQUATIONS

LIST OF TABLES

LIST OF SYMBOLS

ρ	Density (kg/m^3)
$\vec{v}$	Velocity (m/s)
p	Pressure (Pa)
$\vec{g}$	Gravity (m/s^2)
α	Volume fraction
m_{pq}	Transfer of mass from phase p to q
m_{qp}	Transfer of mass from phase q to p

ABSTRACT

Entrainment is the process of movement of one fluid in another due to the presence of a driving force. Entrainment process can be seen both in natural and artificial events. Cyclonic winds and weather storms include stratified layers of air and water phases. In the present thesis, a three phase system is considered, consisting of two immiscible liquids and a gas bubble. Numerical studies have been carried out to find out the strength of inertial entrainment before detachment of bubbles. Wide range of size of air bubbles are considered as the driving factor for entrainment.

The objective of the present work is to study how bubble diameter effects the height of entrainment and flow patterns. Two different fluid pairs are considered and their mutual merits and demerits for controlling entrainment are discussed. 2D numerical analysis is done using commercial CFD software Fluent in ANSYS.

Keywords: Entrainment, Liquid-liquid, Volume of Fluid (VOF), Finite Volume Method (FVM), Three Phase Flow, Numerical modeling.

CHAPTER 1:

INTRODUCTION AND LITERATURE REVIEW

In this chapter, the problem has been explained in detail along with the basic principle behind the phenomena and its occurrence. The practical uses of the phenomena have been discussed along with the literature review covering the work that has already been done. The gaps in the literature have been pointed out and the aims and objectives of the present work, in accordance with the gaps found, have been listed.

1.1 INTRODUCTION

Entrainment is the process of movement of a one fluid in another fluid due to the presence of a driving force. It is a multiphase phenomenon. When a fluid goes from one medium to another medium it takes the prior medium with it due to the drag force present within themselves. In general various shape and sizes of air bubbles are the reason for entrainment. As the bubbles move up it takes the denser medium into the rarer medium with it. The denser medium doesn't break off the rarer medium due to the surface tension of the air bubble.

Here work has been done mainly on inertial entrainment caused by forces of inertia. The dragging of denser medium into rarer medium with the help of air bubbles is known as inertial entrainment phenomena. As the density of air is less than other two fluid mediums; if we inject an air bubble inside a denser medium it goes up due to the buoyant force. As it crosses the intersection of two mediums the denser medium tries to enter into the rarer medium. The air bubble gradually gets compressed due to the pressure experienced by the liquid medium. Due to gravity, the denser medium gets detached from the air bubble and goes down due to its weight and the bubble goes up.

We come across the entrainment phenomena in many of our day to day works. It includes natural as well as artificial processes. Some natural events of entrainment are; mixed layers of air and water phases in cyclonic winds and weather storms. By

calculating the strength of entrainment we can find out the damage caused by a cyclonic storm. Jet pumps are used to pump out the water from flooded compartments of a ship during a leakage. It is an example of use of entrainment in artificial processes. Entrainment is also used to remove non-condensable gases from a condenser to maintain the condenser vacuum in a power plant. Strong entrainment are used to mix two liquids by gas bubble injection process in industries. In nuclear power plants the non-condensable gases form bubbles and causes entrainment which is an important safety issue. So, we saw that entrainment is a very common phenomenon. So, to understand the principle laws behind it will come handy.

1.2 LITERATURE REVIEW

Entrainment phenomena has been a main topic of interest among current as well as old researchers. A lot of research work has been done on this to understand the various parameters affecting the strength of entrainment. Various experiments, analytical and numerical studies has been carried out in this matter.

Liu et al. (2014) have examined the interaction of clay minerals in flotation. The study is finished both pipe water and saline water. The entrainment of clay minerals in flotation is undesired thus the study is done to diminish the entrainment. The outcome is that saline water prompted higher entrainment rate than faucet water. Of the diverse sorts of clay minerals, Kalonite Q38 indicated higher entrainment. Li et al. (2014) have examined the entrainment behaviour of sericite in microcrystalline graphite flotation. Here as well, the point was to decrease the rate of entrainment. Both with and without microcrystalline graphite sericite were tested. The graphite was found to have high effect on the phenomenon. Oka et al. (2014) did work to test the entrainment properties of horizontally spreading ceiling jet. The results obtained are real helpful in fire and

safety rescue missions. Cristofano et al. (2014) have dealt with gas entrainment onset conditions in unsteady free surface vortices. They have utilize a particularly constructed gas entrainment test area for the same. Roy et al. (2013) have researched the perception of air entrainment by plunging jet. The reason for entrainment is found as development of air sheath. In beat stream, Wang et al. (2013) have proposed a numerical model for the drop-entrainment. The impact of parameters have been researched and examined. Wang et al. (2013) have again researched the wave and drop entrainment tentatively. Kulkarni and Patwardhan (2013) have examined the sensation of gas entrainment in blended tanks by CFD displaying. The onset conditions have been explored. In a diesel engine, crevice soot entrainment have been computationally contemplated by Tan et al. (2013). The discoveries have been utilized to stretch the life of engines. Brouilliot and Lubin (2013) have numerically mimicked entrainment of air in a plunging fluid jet. They have added to the numerical model for traditional VOF- PLIC model. They have likewise utilized LES turbulence model. In fluid frameworks, Shahrokhi and Shaw (1994) have researched the start of drops by cluster gas tumult. Their criteria was to minimize the fine drop development. The work is exploratory in nature. Greene et al. (1991) have created investigative model for incitement of air pocket entrainment between stratified fluid layers. The entrainment efficiencies have been computed. Greene et al (1988) have likewise examined the quality of the entrainment by measuring the volume of entrained fluid. Distinctive fluid sets were utilized as a part of trial runs.

1.3 GAPS IN THE LITERATURE

From the literature review, it can be seen that very few attempts has been made on three phase (liquid-liquid-gas) inertial entrainment problems to the best of the author's knowledge. Even if few experiments has been done in entrainment phenomenon but no

numerical simulation of three phase entrainment has been done yet to the best of the author's knowledge. Furthermore no attempts has been made to formulate the dependency of various factors on entrainment.

Therefore a rigorous investigation is required for three phase entrainment phenomena both experimentally and numerically.

1.4 AIMS AND OBJECTIVE

Here the basic aim is to numerically study the inertial entrainment phenomena, to quantify the strength of the entrainment of the denser medium in terms of height. The other objectives are to investigate the effect of liquid properties, shape and size of the container, bubble size, etc. on the phenomena of inertial entrainment. Another aim is to capture the variation of velocity of the bubble in different stages of entrainment. Due to the limitation in time and resources required for experimentation, one can go for numerical investigation on inertial entrainment phenomena.

CHAPTER 2:

PROBLEM STATEMENT

In this chapter, the problem has been extensively described with schematic representation and boundary conditions. For the better understanding of the phenomena, different cases related to his problem have been considered which are categorically described in this chapter.

2.1 PROBLEM DESCRIPTION

As shown in Figure 2.1, the vertical container contains two immiscible fluids (Fluid 1 and Fluid 2) of different densities. Fluid 1 (denser medium) occupies the bottom half of the tank and Fluid 2 (lighter medium) occupies the rest of the tank. As the two fluids are immiscible and densities are different, they will form a stratified liquid layer of a common interface between them.

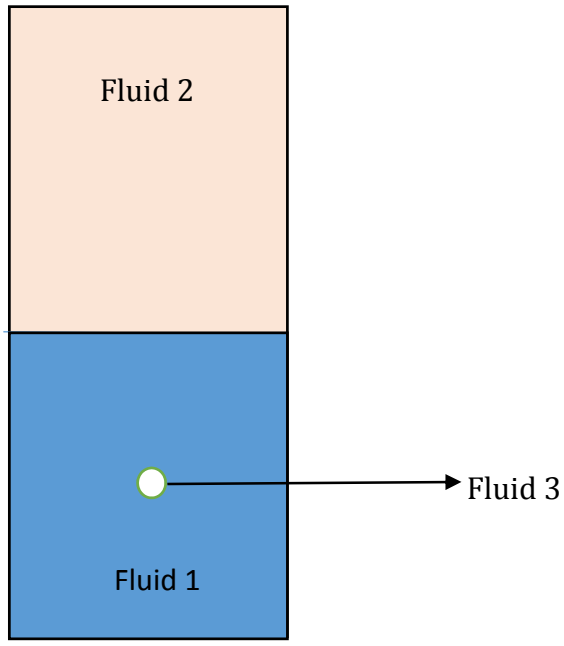

Figure 2.1: Schematic diagram of the problem statement.

First an air bubble is injected in the lower denser medium (Fluid 1). Due to the buoyancy force acting on the bubble, it gradually rises up and gains momentum. Some drag force acts on the bubble. As it reaches the interface of two fluid pairs, it goes from

the denser medium to lighter medium. Due to the viscous effects of the fluids and the inertial impact of the bubble, some denser liquid breaks off from its bulk and enters into the lighter medium with the air bubble. As a result, entrainment of the heavier phase into the lighter phase occurs due to the inertial impact. Then it travels up to some height in the lighter medium due to the momentum provided by the gas bubble. Due to the gravity force and viscous effect of the lighter medium, heavier medium again detaches from the bubble and forms a drop of the heavier liquid. It will move up to certain distance in the upward direction due to inertia effect and then starts to fall. Here the problem is to identify the distance from the interface where the velocity of the drop of the heavier medium becomes zero and starts to fall. The top of the container is open to atmospheric pressure (i.e. the free surface of the lighter liquid is exposed to the atmospheric pressure) while other sides are closed by wall. In the wall no slip and no penetration (U_x and U_y) boundary condition have been used. Different cases has been considered by varying the parameters related to the problem for the better understanding of the physics lying behind the phenomena. These cases are categorically discussed below.

2.2 EFFECT OF BUBBLE SIZE ON THE ENTRAINMENT HEIGHT

The effect of bubble size on the strength of the entrainment has been investigated by measuring the entrainment height. Corresponding results are discussed in the results section. Effect of the bubble size on the phenomena has been studied separately for different fluid pairs as shown below.

2.2.1 Effect of Bubble Size on the Kerosene-Water Fluid Pair: Here, water is taken as the denser medium (Fluid 1) and kerosene is taken as the lighter medium (Fluid 2). Considering this fluid pair, the height of maximum entrainment has been calculated

by varying the size of the bubble. The variation velocity of the bubble has also been plotted against time for each of the above cases.

2.2.2 Effect of Bubble Size on the Diesel-Water Fluid Pair: Here, water is taken as the denser medium (Fluid 1) and diesel is taken as the lighter medium (Fluid 2). Considering this fluid pair, the height of maximum entrainment has been calculated by varying the size of the bubble. The variation velocity of the bubble has also been plotted against time for each of the above cases.

2.3 EFFECT OF FLUID PAIR

In this section the effect of fluid pair on the height of entrainment and velocity of air bubble has been investigated by varying the fluid pair.

2.3.1 Effect of Fluid Pair on Height of Entrainment: The effect of two different fluid pairs on the maximum height of the entrainment has been investigated and the corresponding results are provided in the results section.

2.3.2 Effect of Fluid Pair on the Velocity of Air Bubble: The effect of two different fluid pairs on the velocity of air bubble has been investigated and the corresponding results are provided in the results section.

CHAPTER 3:

METHODOLOGY

Here in this chapter, the methodology to tackle the present problem is extensively explained. It can be solved both experimentally and using numerical methods. To numerically simulate the problem, Finite Volume Method (FVM) with Volume of Fluid Model (VOF) has been used. 2D unsteady analysis have been performed to capture the flow regime (flow structure) properly.

Numerical method has been used to simulate the phenomenon of inertial entrainment. Commercial CFD software Fluent in ANSYS 15 has been used to numerically simulate the problem.

3.1 NUMERICAL CALCULATION

In the present study, Volume of Fluid (VOF) model has been used to numerically simulate the two-phase flows in an upright pipe. The VOF model is used to solve the multiphase problem that involves mixtures of two or more immiscible fluid by continuity and momentum equation and keeps the record of the volume fraction of each fluid throughout the whole system. It can be quite accurately used for both 2D as well as 3D geometry. Tracking large bubbles in liquid mixture and tracking of steady or transient fluid-gas interface are some of its major application. It depends on the fact that two or more phases don't interpenetrate. For modelling of phases it adds additional volume fraction functions to the computational cells of control volume. So, the volume fraction of each fluid comes into play to determine field variables and properties. Based on all above mentioned advantages for simulating a multiphase flow, VOF was used. For turbulence modelling, standard k-ε model is used. The standard k-ε is the most commonly used turbulence model. It is robust and reasonably precise for a wide range of application .For near wall treatment standard wall function has been used.

3.2 GOVERNING EQUATIONS

The equations that are used by fluent to solve the problem are continuity (**Equation *3.1***), momentum (**Equation *3.2***) and volume fraction (**Equation *3.3***) equations. Since Volume of fluid model is used, the momentum equation is the same for all the phases, and a weighted average is used for the properties. Turbulence kinetic energy (**Equation *3.4***) and Turbulence dissipation energy (**Equation *3.5***) are used for turbulence modelling.

$$\nabla.(\rho\vec{v}) = 0$$

Equation 3.1: Continuity equation

$$\frac{\partial(\rho\overrightarrow{v})}{\partial t} + \nabla.(\rho\vec{v}\vec{v}) = -\nabla p + \nabla\left(\mu(\nabla\vec{u} + \nabla\vec{u}^T)\right) + \rho\vec{g} + \vec{F}$$

Equation 3.2: Momentum equation

$$\frac{1}{\rho_i}\left[\frac{\partial(\alpha_i\rho_i)}{\partial t} + \nabla.(\alpha_i\rho_i\vec{v}_i)\right] = \sum_{i=1}^{n}(\dot{m}_{pq} - \dot{m}_{qp})$$

Equation 3.3: Volume fraction equation

Turbulence modelling using *k-εpsilon* equation

Turbulence kinetic energy k equation is used to determine the turbulence velocity scale:

$$\frac{\partial}{\partial t}(\rho k) + \frac{\partial}{\partial x_i}(\rho k u_i) = \frac{\partial}{\partial x_j}\left[\left(\mu + \frac{\mu_i}{\sigma_k}\right)\frac{\partial k}{\partial x_j}\right] + G_k + G_b - \rho\varepsilon - Y_M + S_k$$

(Equation 3.4)

and Turbulence dissipation energy ε equation is given by

$$\frac{\partial}{\partial t}(\rho\varepsilon) + \frac{\partial}{\partial x_i}(\rho\varepsilon u_i) = \frac{\partial}{\partial x_j}\left[\left(\mu + \frac{\mu_i}{\sigma_\varepsilon}\right)\frac{\partial\varepsilon}{\partial x_j}\right] + C_{1\varepsilon}\frac{\varepsilon}{k}(G_k + C_{3\varepsilon}G_b) - C_{2\varepsilon}\rho\frac{\varepsilon^2}{k} + S_\varepsilon$$

(Equation 3.5)

Where,

G_k = Generation of turbulence kinetic energy due to the mean velocity gradients.

G_b = Generation of turbulence kinetic energy due to buoyancy.

$C_{1\varepsilon}, C_{2\varepsilon}$ & $C_{3\varepsilon}$ = constants. σ_k & σ_ε = Turbulent Prandtl numbers.

S_k & S_ε = User-defined source terms.

$\mu_t = \rho C_\mu \frac{k^2}{\varepsilon}$ = The turbulent viscosity.

3.3 GEOMETRY AND GRID SPECIFICATIONS

First the geometry has been created using in fluent section of ANSYS workbench. First a square sketch of dimensions 70 mm × 300 mm is created in XY plane by the sketching tool. Then using that sketch a surface was generated by surface from sketches tool.

After generating the geometry file grids have been created using meshing workbench. First the geometry file was attached and using mesh insert method mesh was generated by triangle method. Then the size of the mesh size is increased to make it fine. The two dimensional grid created contains 19592 cells, 29635 faces, 10044 nodes and only one partition.

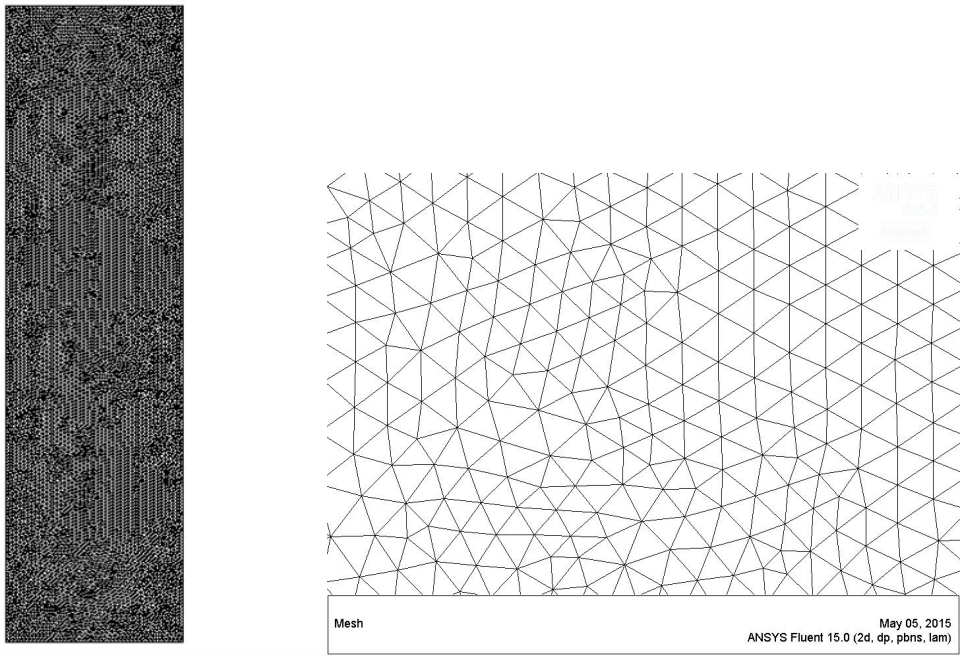

Figure: 3.1: Grid using triangular meshing and its zoom-in view

3.4 BOUNDARY CONDITIONS

The boundary conditions used for the problem are discussed here. The left and right edge of the two-dimensional container are given the boundary condition wall. The top of the container is set as pressure outlet with gauge pressure set at 0. At pressure outlet i.e. top of the container the turbulence parameters are given as intensity and hydraulic diameter and the intensity value was set as 5%.

3.5 SOLUTION METHODS

Here, 2D planar flow is considered with transient phenomena. Pressure based solver is used. Velocity formation is kept absolute. As the system is vertical, gravity is also considered. Under Models Volume of Fluid (VOF) was selected in multiphase and three Eulerian phases are selected. For turbulence modelling, standard k-ε model is used. Then in material section water-liquid, kerosene or diesel were selected based on

required fluid pair. Water was selected as primary phase and air as secondary phase. Kerosene or diesel are selected as secondary phase. In Solution Methods we used PISO (Pressure implicit with splitting of operator) under pressure-velocity coupling scheme as it is strongly suggested for cases involving a transient flow, especially in case of large time step. As the mesh is not distorted, skewness and neighbour relaxation factors are set to unity. Under spatial discretization, Least Square Cell Based Gradient has been used. In this scheme, PRESTO for Pressure, GEO- CONSTRUCT for volume fraction have been used. Moreover, first order upwind for both turbulent kinetic energy and Turbulent Dissipation Rate and second order upwind for momentum have been used. In Transient Formulation scheme, first order upwind is used. Then solution was initialised using standard initialisation process computing from all zones. After solution initialization we marked volume using the tool adapt-region for patching different phases inside the container volume.

Table 3.1: Co-ordinates for marking shapes to adapt region volumes

Shapes	**Input Coordinates**
Quad	X Min: 0.00 m X Max: 0.07 m Y Min: 0.15 m Y Max: 0.30 m
Circle	X centre: 0.035 m Y Centre: 0.07m Radius: 0.0055, 0.006, 0.0075 etc.

Then using patching tool kerosene or diesel was patched in the hexahedron and air was patched in the circle with volume fraction 1.

The following figure shows the density contour of the mixture with 5 levels after patching.

Figure: 3.2 Initial density contour of the mixture after patching

3.6 RESIDUALS

Under Residuals, the Convergence criteria for all the field variables (continuity, *x*-velocity, *y*-velocity, *k*, and ε) are set to 1*e*-06. Time stepping method is used as fixed type. The time step size is used as 0.00001 sec and maximum number of iteration per time step is set to 40. Reporting interval and profile update interval is set to unity. The case and date file are auto-saved with a regular interval of 0.05 sec.

3.7 VALUES OF PARAMETERS FOR SIMULATION

- Turbulent kinetic energy $k = 3.260327 \times 10^{-12}$ m^2/s^2 and Turbulent dissipation rate $\varepsilon = 1.547478 \times 10^{-16}$ m^2/s^3.
- The fluid properties were set as: Density of water = 998.2 kg/m^3, viscosity of water = 0.001003 Pa-s, density of air = 1.225 kg/m^3, viscosity of air = 1.7894 ×

10^{-5} Pa-s, density of Kerosene = 780 kg/m^3, viscosity of Kerosene = 0.0024 Kg/m-sec, density of diesel = 730 kg/m^3, viscosity of diesel = 0.0024 Kg/m-sec.

- Values of the model constants: $C_{1\varepsilon} = 1.44, C_{2\varepsilon} = 1.92, C_{3\varepsilon} = 0.09, \sigma_k = 1 \,\&\, \sigma_\varepsilon = 1.3$.

CHAPTER 4:

Results & Discussions

At first, the methodology has been validated by comparing with the previous experimental results. The results obtained by numerical simulation have been discussed in details. Results for each of cases considered in Chapter 2 are shown and elaborately discussed here.

4.1 GRID INDEPENDENCE TEST

Grid independence test is a must and important test for all numerical simulations. The results obtained should be independent of meshing method used and the grid size. To perform this test, four different mesh arrangements (number of nodes, grid size) have been considered and simulations are performed for each. Then the density contours and maximum height of entrainment for the 4 different mesh files are compared to check the grid independence. The number of nodes for this four different mesh arrangements are 9952, 10044, 15389, 22387 respectively.

4.1.1 Comparison of Maximum Height of Entrainment: The following Table 4.1 shows the variation of maximum height of entrainment with number of nodes. From the Table 4.1 and Figure 4.1 it is clear that the maximum height of the entrainment does not vary so much with the selected grid size. Therefore a mesh structure with 10044 number of nodes has been selected to show the numerical results for all the cases.

Table 4.1: Maximum height of entrainment by varying the number of nodes in the mesh

Number of Nodes	Height of Entrainment (in mm)
06246	127.941
10044	125.981
15389	132.980
22387	131.863

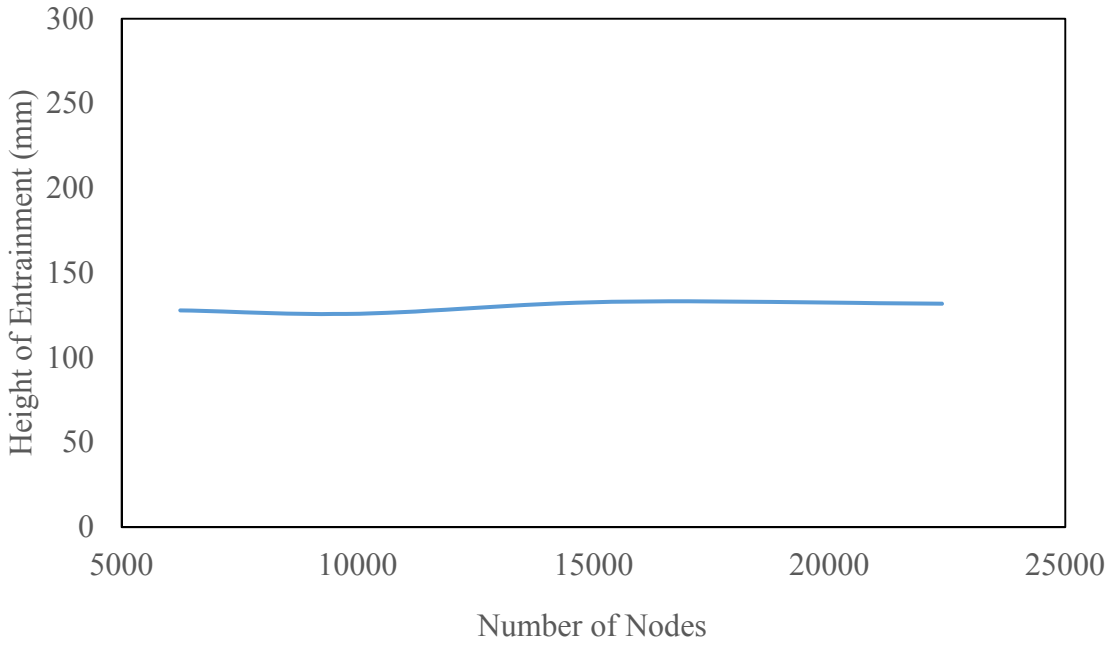

Figure 4.1: Variation of maximum height of the entrainment with number of nodes for the fluid pair: Diesel-Water and Bubble Diameter: 11 mm

4.1.2 Comparison of Contours at Maximum Height of Entrainment: The density contours of all 4 grids at maximum height of the entrainment is given below for comparison. From the Figure 4.2 we can see that the density contour also does not vary much with the selected grid size.

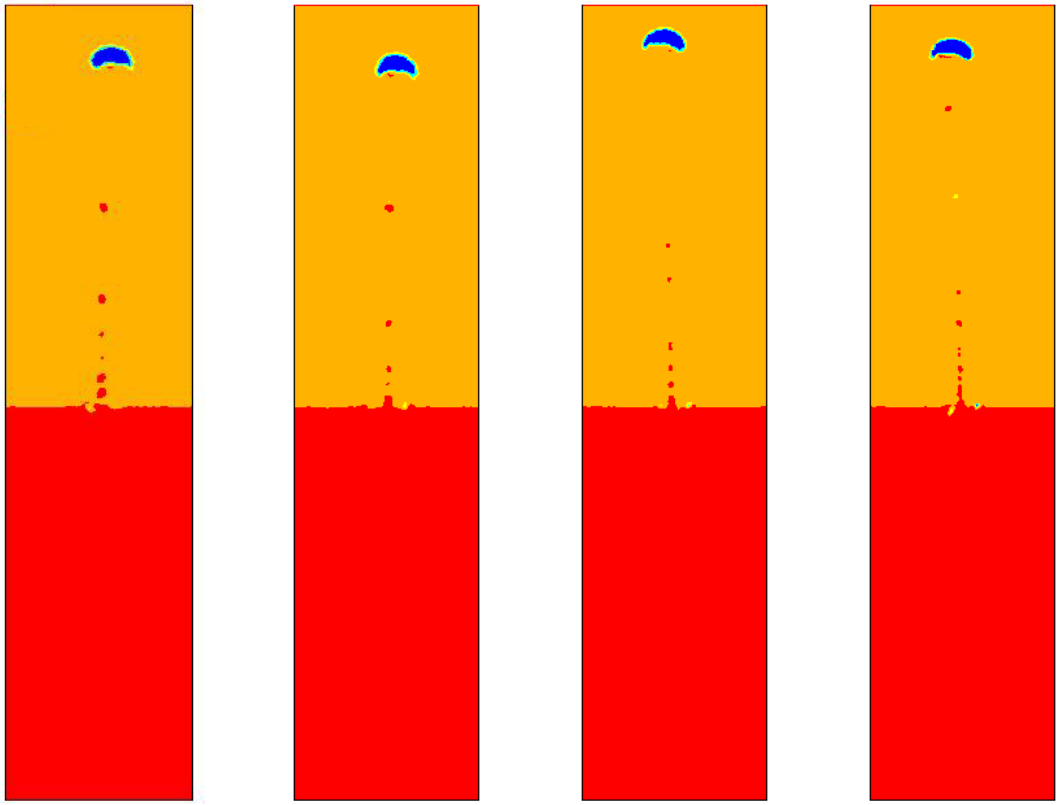

N = 6246 N = 10044 N = 15389 N = 22387

Figure 4.2: Comparison of Density Contours at Maximum Height of Entrainment

Where N = Number of Nodes

4.2 VALIDATION OF THE NUMERICAL SCHEME

At first, the methodology has been validated by comparing the results obtained from numerical analysis with previous experimental results obtained by Verma et al. (2014). The boundary conditions and other parameters are also taken same as that of experimental setup. For the present validation, fluid pair is considered as diesel-water and a container with rectangular cross-section (70 mm × 300 mm) is considered. The bubble volume is considered as 7×10^{-7} m^3 (Bubble Diameter is 11 mm) for the present validation.

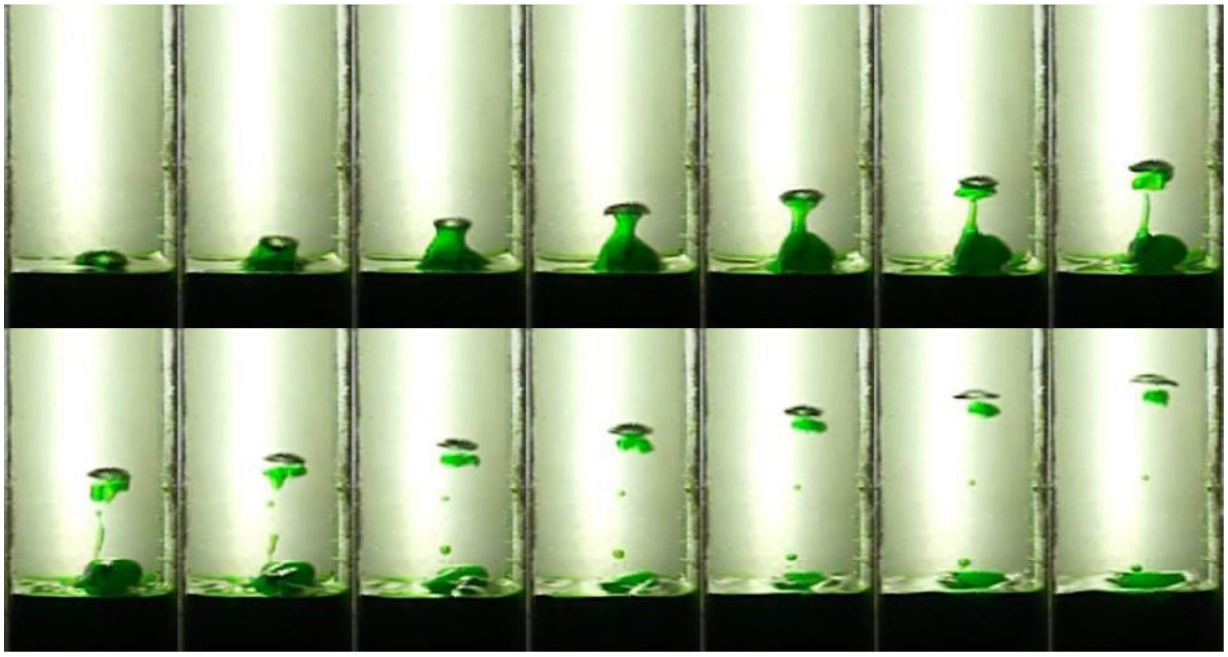

Figure 4.3: Various stages of the entrainment with time step 1/30 sec as obtained by Verma et al. (2014) through experimentation for the fluid pair: Diesel-Water.

The stages of entrainment obtained from numerical simulation are shown below with a time gap of 0.15 seconds starting from time t = 1.05 sec.

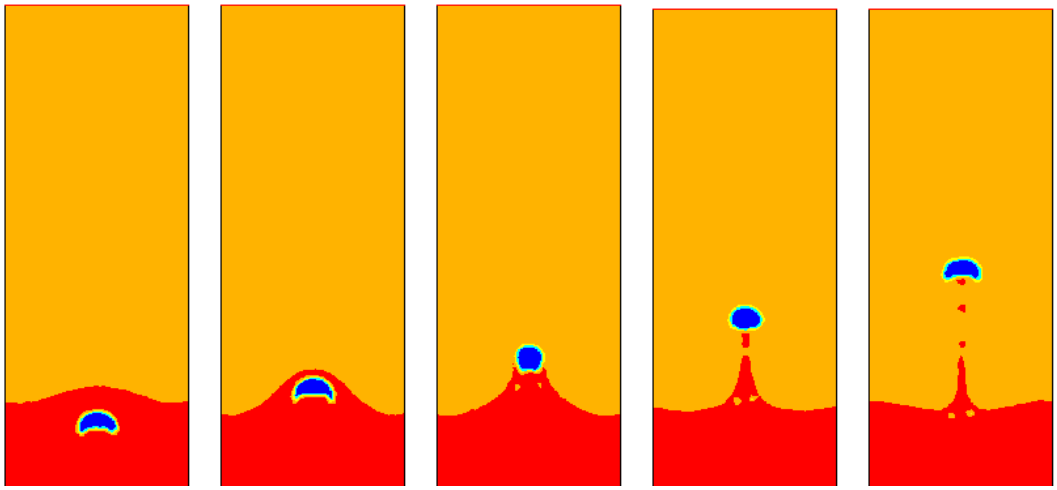

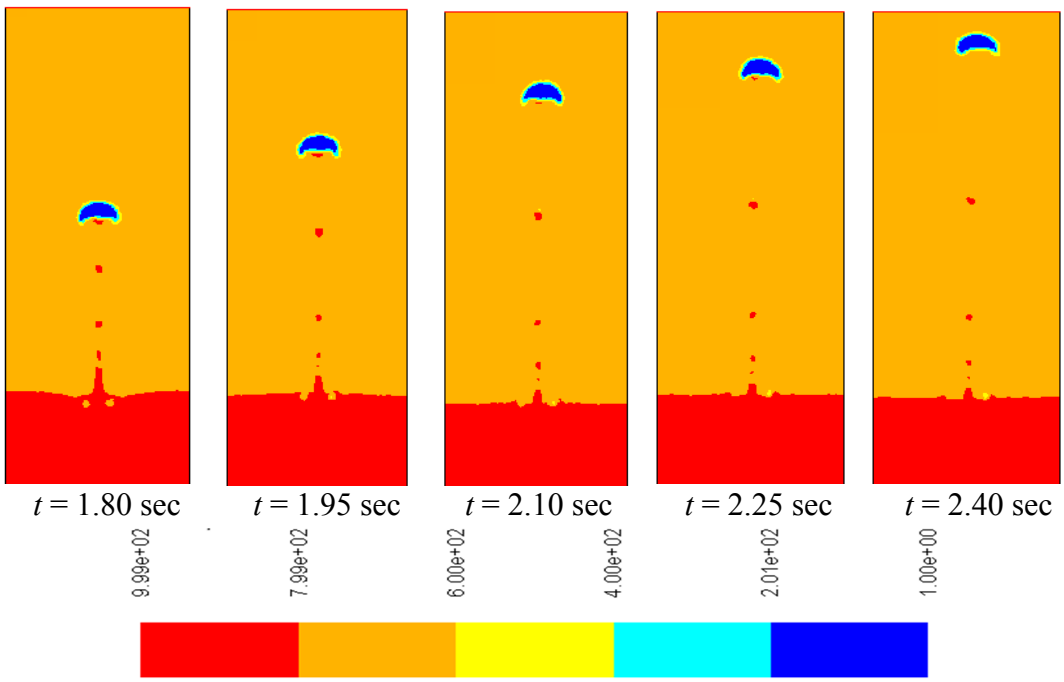

Figure: 4.4: Density contour at various stages of the entrainment with a time interval of 0.15 sec for the fluid pair: Diesel-Water (container size: 70 mm × 300 mm)

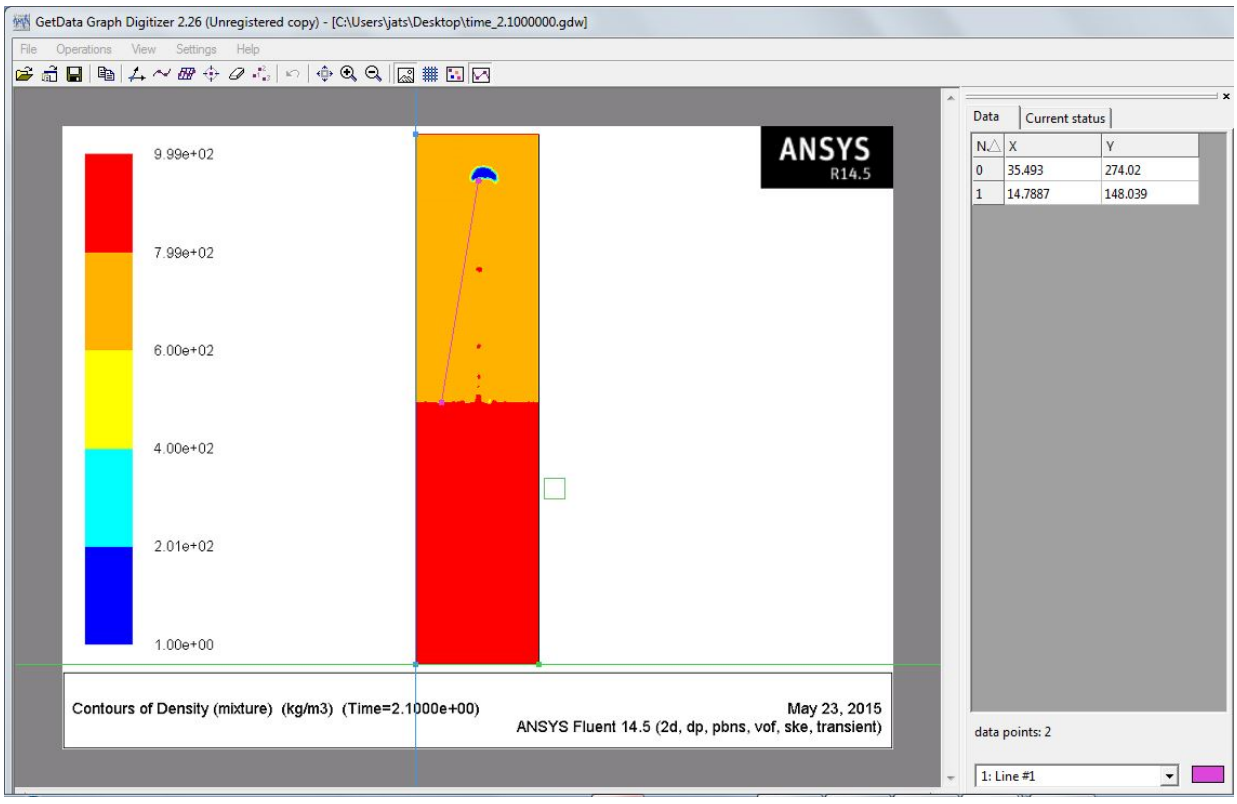

Figure 4.5: Entrainment height calculation using the software: *Get Data Graph Digitizer*

The water medium leaves the air bubble at 2.10 seconds from starting. The maximum height of entrainment can be calculated by using a software (named **Get Data Graph Digitizer** version 2.6). The height of entrainment from base = 274.02 mm. The height of water medium 1 from base = 148.039 mm. Therefore, actual height of entrainment = (274.02-148.039) mm = 125.981 mm. From experiments conducted by Verma et al. (2014), maximum height of entrainment for bubble volume of 7×10^{-7} m^3 (i.e. diameter =11.016 mm) = 0.129086178 m = 129.086 mm. As both the results obtained by numerical and experimental analysis are almost same. Hence it is verified that the numerical simulation scheme followed here is correct and permissible.

4.3 EFFECT OF BUBBLE SIZE ON ENTRAINMENT PHENOMENA

In this section, the phenomena of entrainment for different size (diameter) of the bubble have been represented in several ways to capture the dynamics properly. For every case the container cross-section is 70 mm × 300 mm.

4.3.1 Effect of Bubble Size on Kerosene-Water Pair: The various effects of bubble size on the entrainment phenomena with Kerosene-Water Pair are shown below. These effects have been shown in terms of dependency of flow structure, maximum height of entrainment and bubble velocity on the bubble size as shown below.

4.3.1.1 Effect of bubble size on flow structure: The density contours at various stages of the entrainment with a time interval of 0.3 seconds are shown in Figure 4.6, 4.7 and 4.8 for the bubble diameter 10 mm, 11 mm and 12 mm respectively.

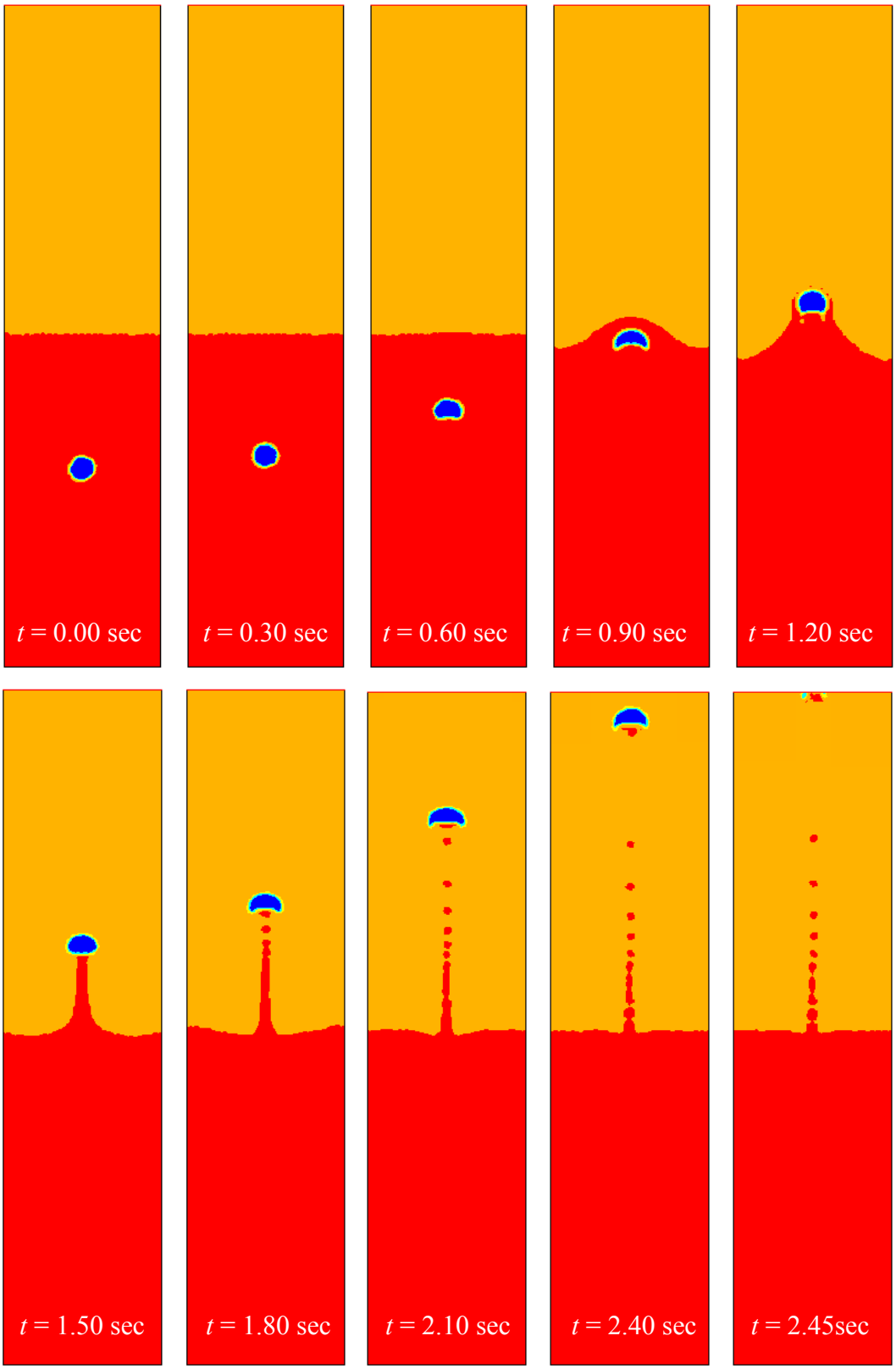

Figure: 4.6: Density contour at various stages of the entrainment for bubble with diameter = 10 mm with a time interval of 0.3 sec for the fluid pair: Kerosene-Water.

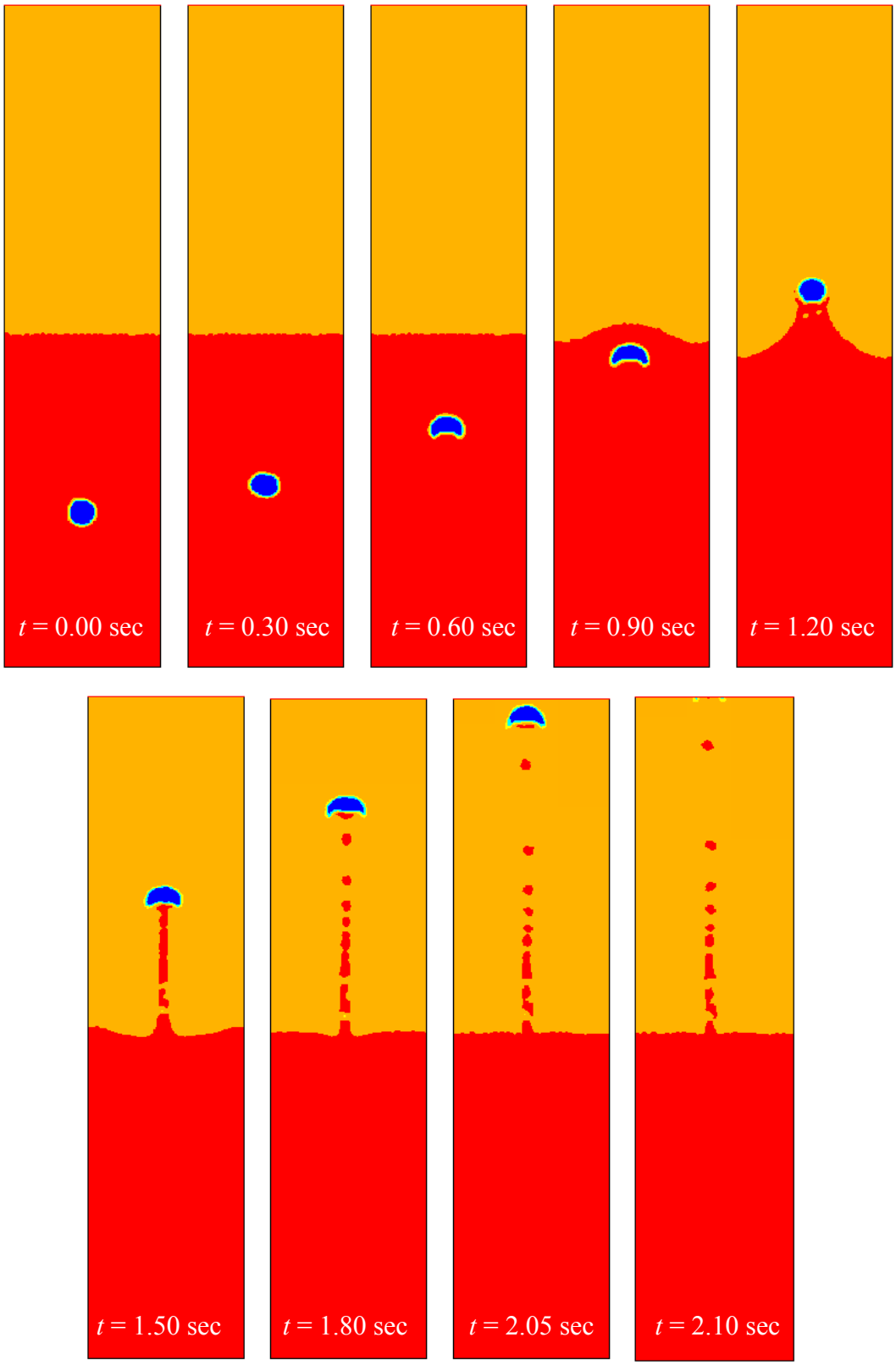

Figure: 4.7: Density contour at various stages of the entrainment for bubble with diameter = 11 mm with a time interval of 0.3 sec for the fluid pair: Kerosene-Water.

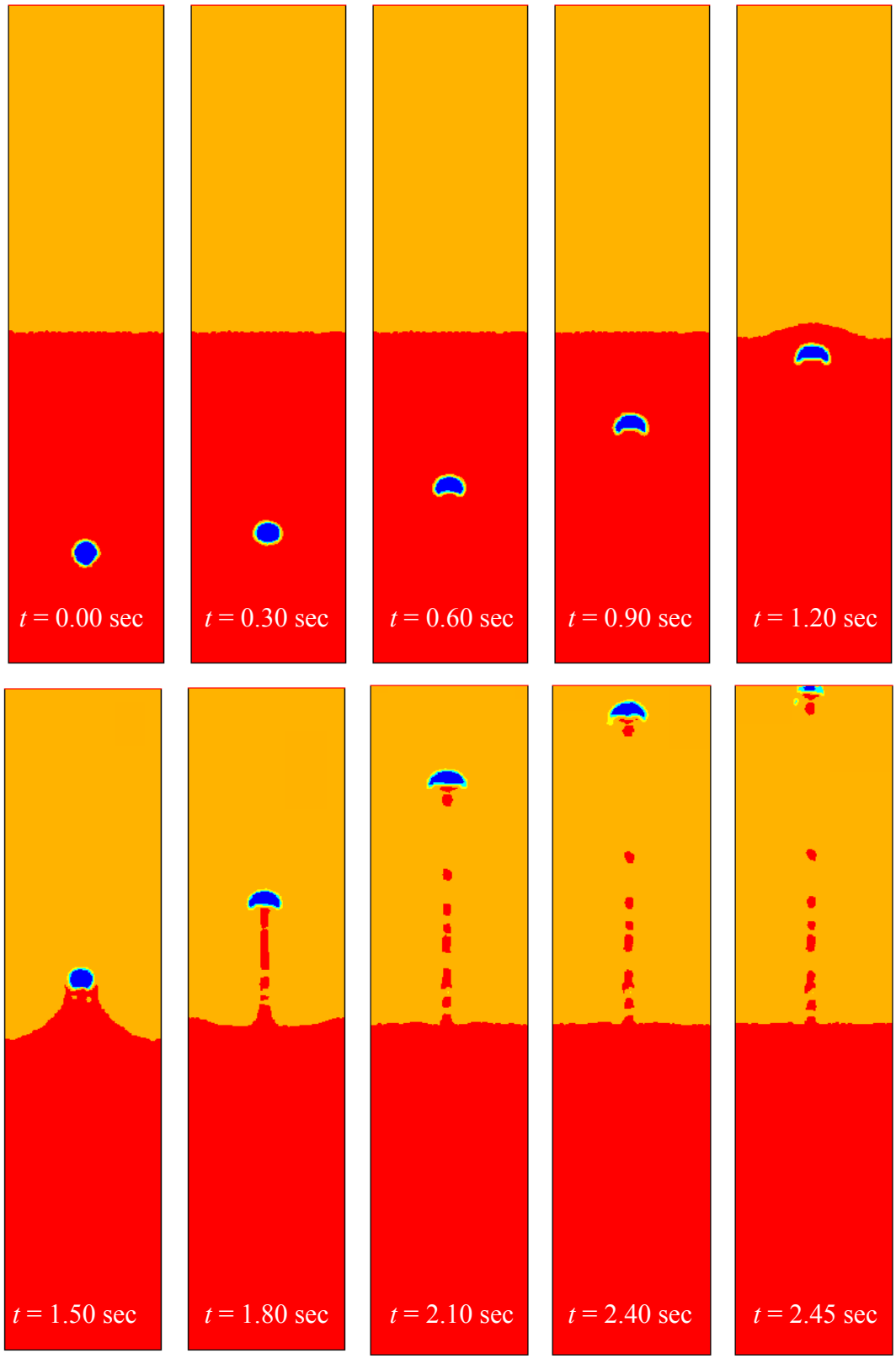

Figure: 4.8: Density contour at various stages of the entrainment for bubble with diameter = 12 mm with a time interval of 0.3 sec for the fluid pair: Kerosene-Water.

4.3.1.2 Effect of bubble size on the maximum height of the entrainment:

The bubble diameter and corresponding height of entrainment in SI units are shown in Table 4.2. Then the graph is plotted between height of entrainment and bubble diameter as shown in Figure 4.9. From the Table 4.2 and the Figure 4.9, it is clear that the height of entrainment is directly proportional to size (diameter or volume) of the air bubble. It is due to the fact that as the size of the bubble increases, the buoyancy force increases, as a result velocity increases and consequently inertial impact on the interface also increases.

Table 4.2: Variation of maximum height of entrainment with bubble diameter for fluid pair kerosene - water

Bubble Diameter (in mm)	Height of entrainment (in mm)
10	150.490
11	164.636
12	187.314

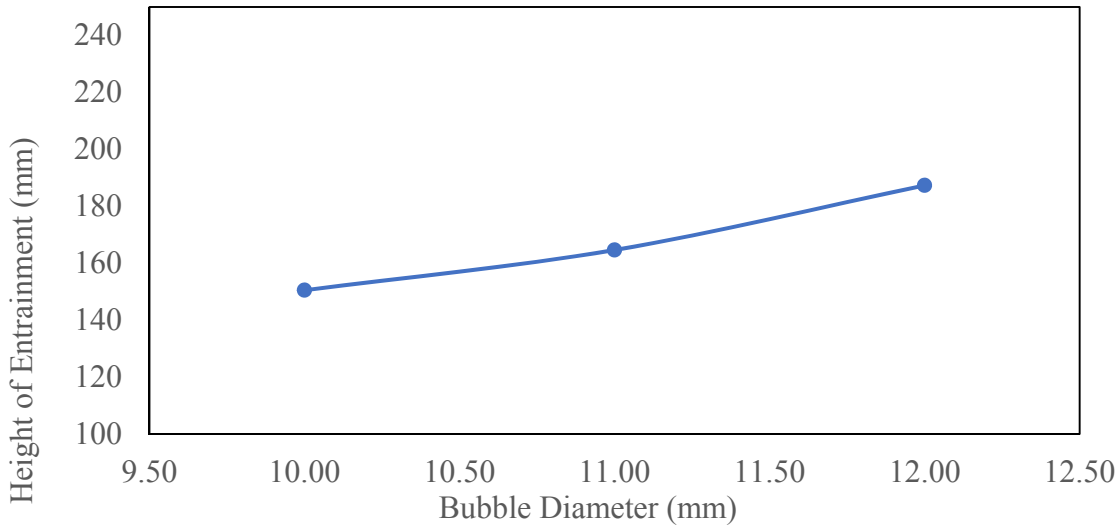

Figure 4.9: Variation of height of entrainment with bubble diameter for the fluid pair kerosene-water

4.3.1.3 Effect of bubble size on bubble velocity: The velocity of bubble at various stages of entrainment is calculated for different size of the bubble. This velocity are then plotted against time. The software **Tech Plot** has been used to find the height through which the bubble moves up in a certain time interval Δt = 0.1 sec. Then the height is divided by the time interval to get the instantaneous velocity of the air bubble. For calculation of bubble's velocity, the following equation has been used.

$$V_{t+\Delta t} = \frac{h_{t+\Delta t} - h_t}{\Delta t} \qquad \textbf{(Equation } \textit{4.1}\textbf{)}$$

Figure 4.10 shows the variation of the velocity of the bubble with time as it moves in the upward direction for different value of the bubble diameter. From the Figure 4.10, it is observed that the velocity of air bubble increases with flow-time. This is because of acceleration due to the force of buoyancy. For all the three cases, the velocity first increases, then becomes constant for a time then again increases with flow time.

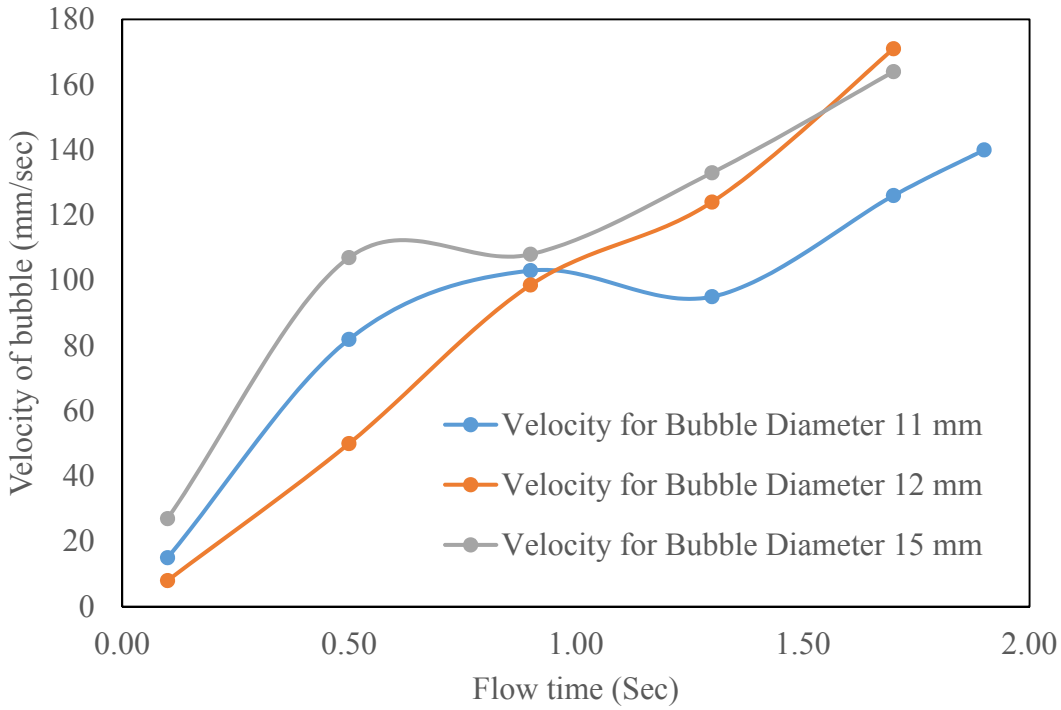

Figure 4.10: Variation of bubble velocity with flow time for fluid pair: Kerosene-Water

4.3.2 Effect of Bubble Size on Diesel-Water Pair: The various effects of bubble size on the entrainment phenomena with Diesel-Water Pair are shown here. These effects have been shown in terms of dependency of flow structure, maximum height of entrainment and bubble velocity on the bubble size as shown below.

4.3.2.1 Effect of bubble size on flow structure: The density contours at various stages of the entrainment with a time interval of 0.3 seconds are shown in Figure 4.11, 4.12 and 4.13 for the bubble diameter 11 mm, 12 mm and 15 mm respectively.

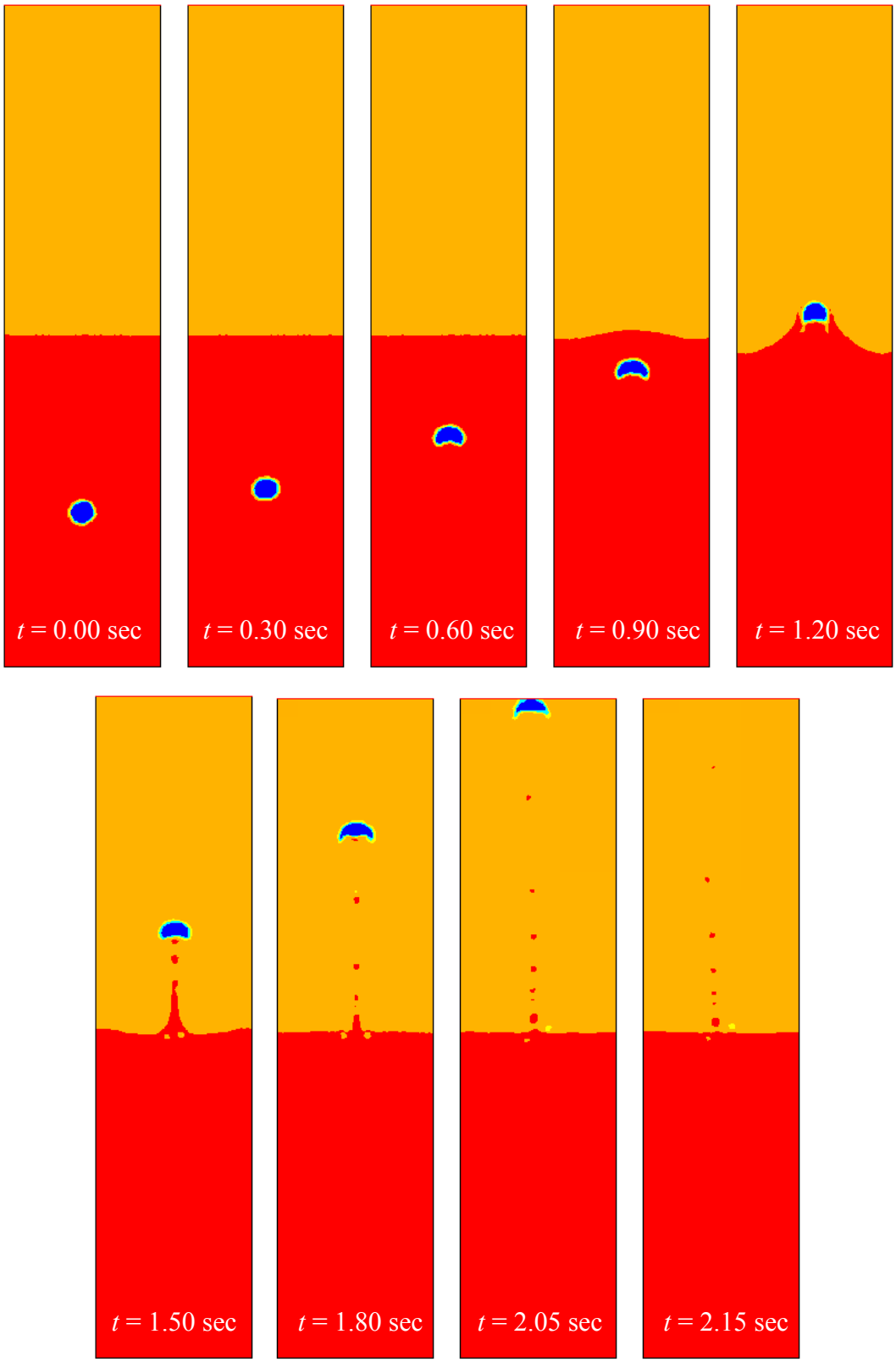

Figure: 4.11: Density contour at various stages of the entrainment for bubble with diameter = 11 mm with a time interval of 0.3 sec for the fluid pair: Diesel-Water.

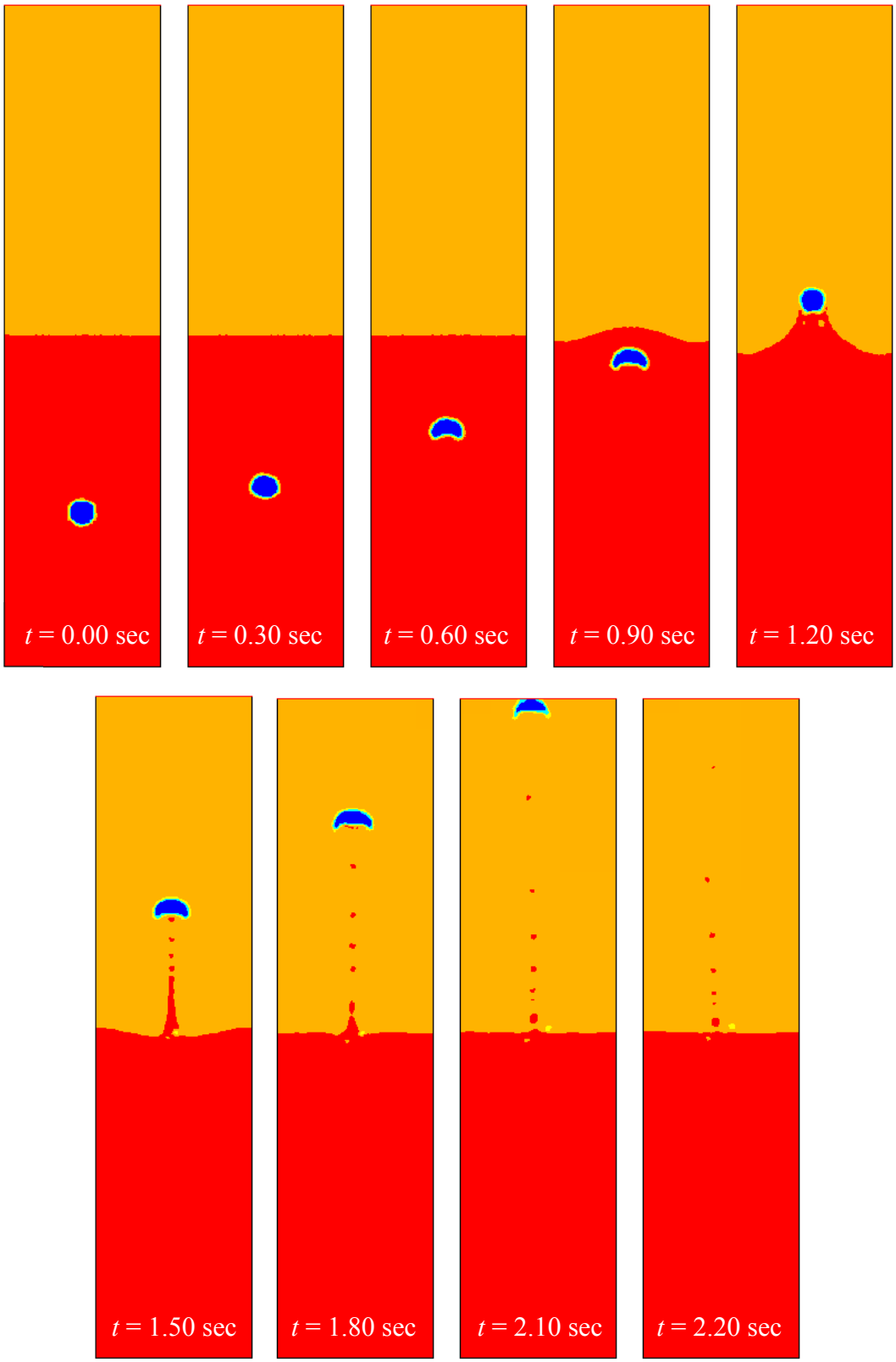

Figure: 4.12: Density contour at various stages of the entrainment for bubble with diameter = 12 mm with a time interval of 0.3 sec for the fluid pair: Diesel-Water.

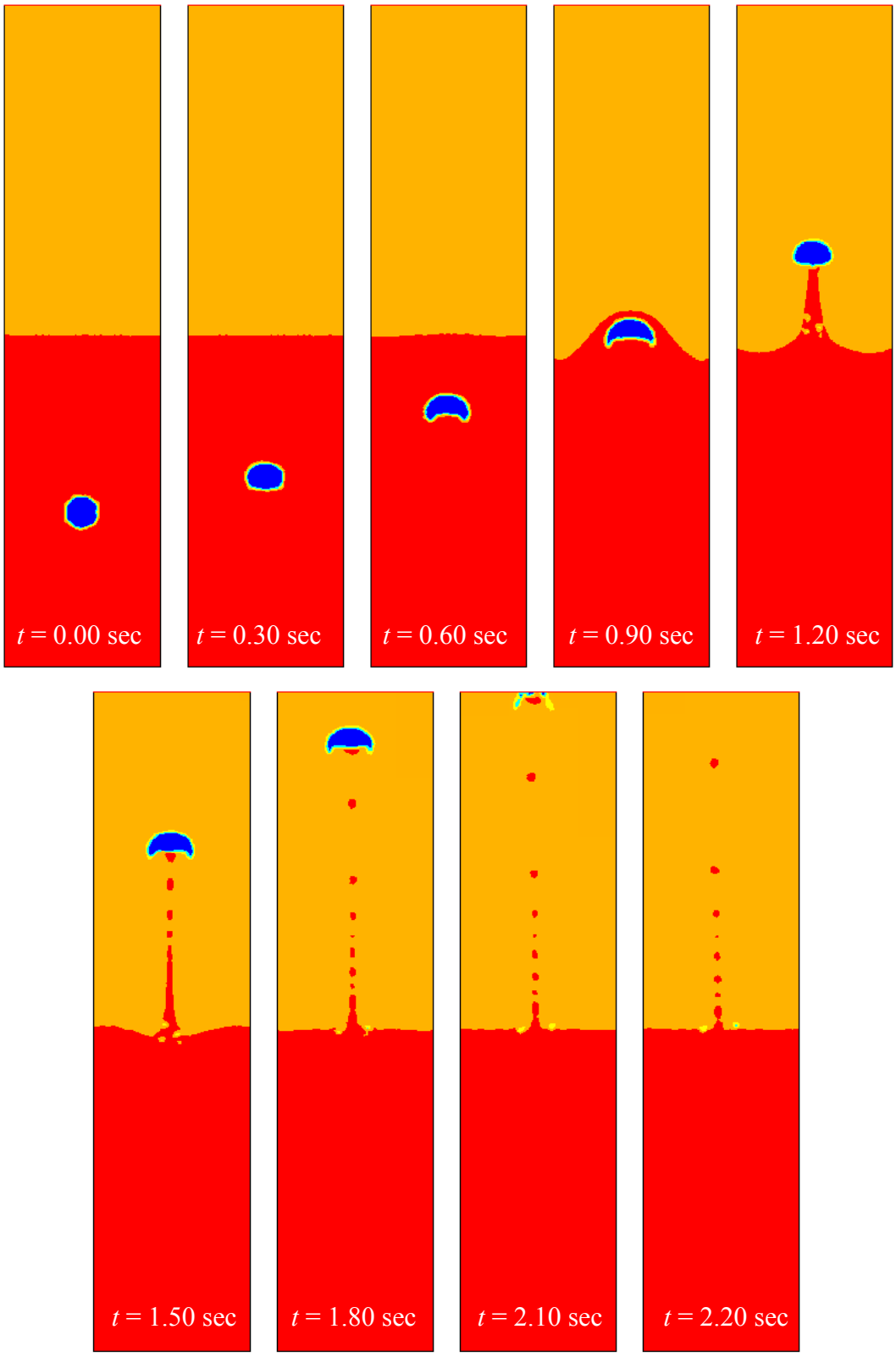

Figure: 4.13: Density contour at various stages of the entrainment for bubble with diameter = 15 mm with a time interval of 0.3 sec for the fluid pair: Diesel-Water.

4.3.2.2 Effect of bubble size on maximum height of entrainment: The bubble diameter and corresponding height of entrainment in SI units are shown in Table 4.3. Then a plot is made between the height of the entrainment and bubble diameter as shown in Figure 4.14. From the Table 4.3 and the Figure 4.14, it is clear that the height of entrainment is directly proportional to size (diameter or volume) of the air bubble. It is due to the fact that as the size of the bubble increases, the buoyancy force increases, as a result velocity increases and consequently inertial impact on the interface also increases.

Table 4.3: Variation of maximum height of entrainment with bubble diameter for fluid pair Diesel – Water

Bubble Diameter (in mm)	Height of Entrainment (in mm)
11	125.981
12	154.258
15	334.126

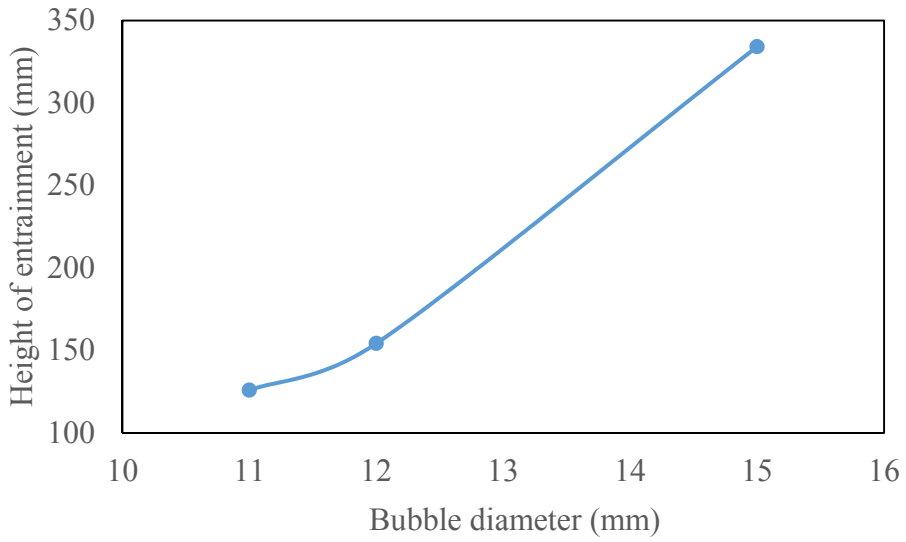

Figure 4.14: Variation of height of entrainment with bubble diameter for the fluid pair Diesel-Water

4.3.2.3 Effect of bubble size on bubble velocity: As explained in Section 4.3.1.3, the velocity of bubble at various stages of entrainment is calculated for different size of the bubble. This velocity are then plotted against time. Figure 4.15 shows the variation of the velocity of the bubble with time as it moves in the upward direction for different value of the bubble diameter. From the Figure 4.15, it is observed that the velocity of air bubble increases with flow-time. This is because of acceleration due to the force of buoyancy. For all the three cases, the velocity first increases, then becomes constant for a time then again increases with flow time.

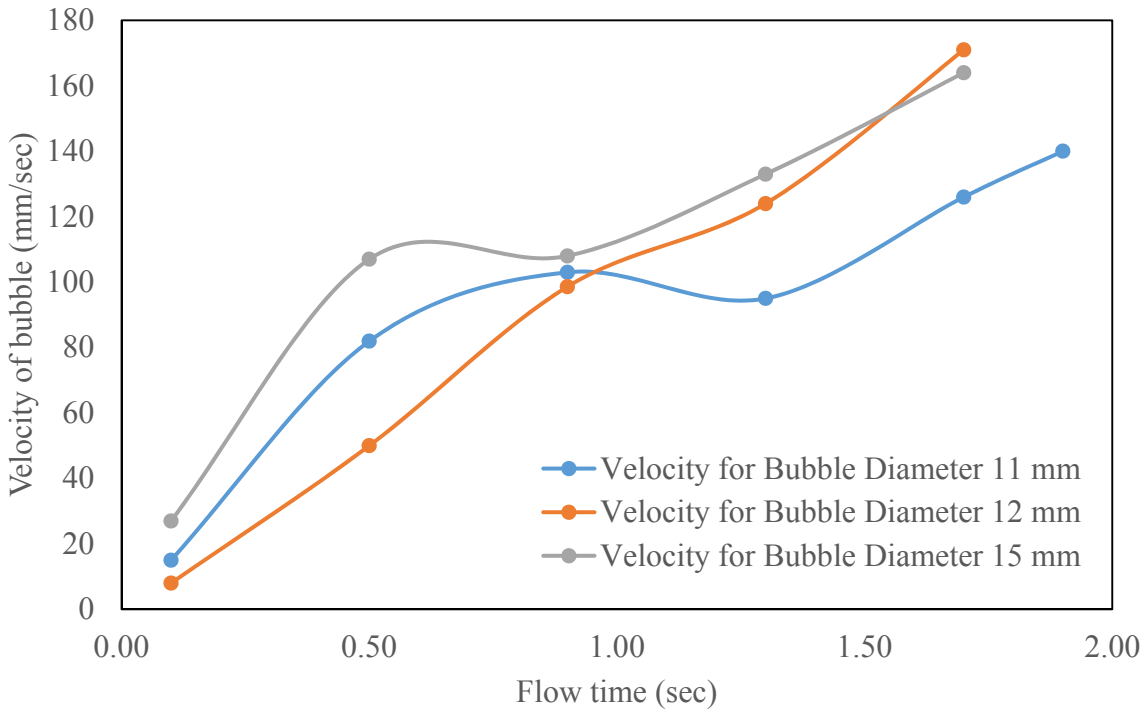

Figure 4.15: Variation of bubble velocity with flow time for fluid pair: Diesel-Water

4.4 EFFECT OF FLUID PAIR ON ENTRAINMENT PHENOMENA

Basically in this section the effect of fluid properties on the inertial entrainment phenomena have been extensively discussed. To get the effect of fluid pair properties, two different fluid pairs have been considered and the study has been repeated.

4.4.1 Effect of Fluid Pair on the Height of Entrainment: The effect of fluid pairs on the height of entrainment is graphically shown in Figure 4.16. From the Figure 4.16, it can be observed that the height of entrainment of kerosene-water fluid pair is greater than that of the diesel-water pair for any particular size of bubble. It is also noticed that the slope with which the height of entrainment increases with the bubble diameter is larger for diesel-water pair.

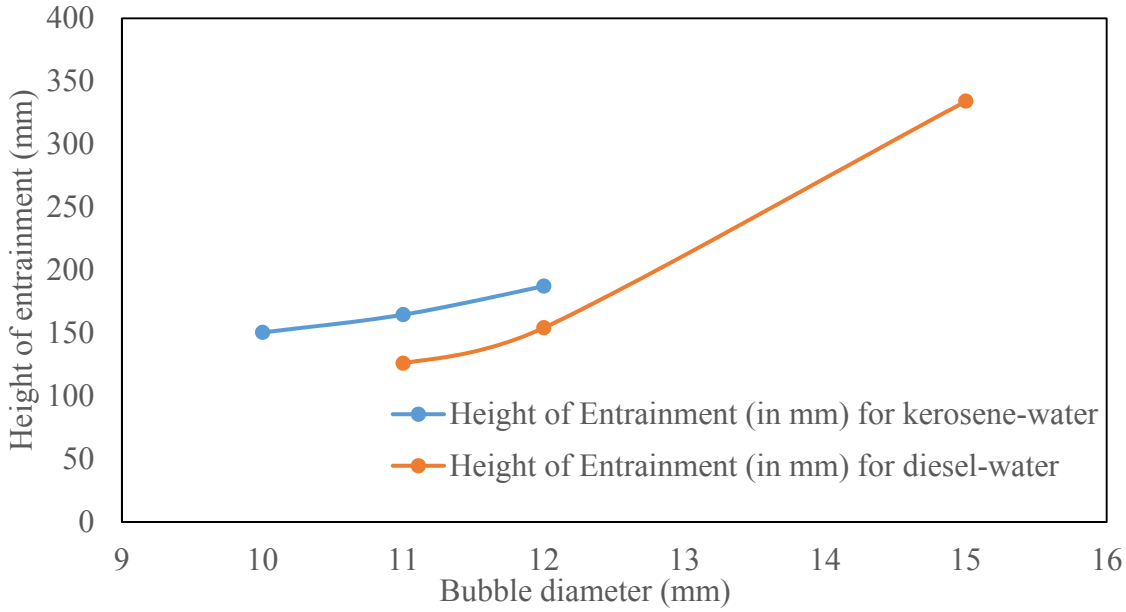

Figure 4.16: Variation of entrainment height with bubble diameter for the two fluid pair

4.4.2 Effect of Fluid Pair on the Velocity of Air Bubble: The velocities of air bubble are plotted against time for both the fluid pairs in a same reference frame and for the same size of the bubble (diameter = 11 mm) as shown in the Figure 4.17. A

comparison has been made between these two plots in Figure 4.17. It is observed that for both the fluid pairs, the velocity of air bubble increases with flow time. For kerosene-water pair, the velocity increases monotonously while for diesel-water pair, it increases then becomes constant for some time then again increases.

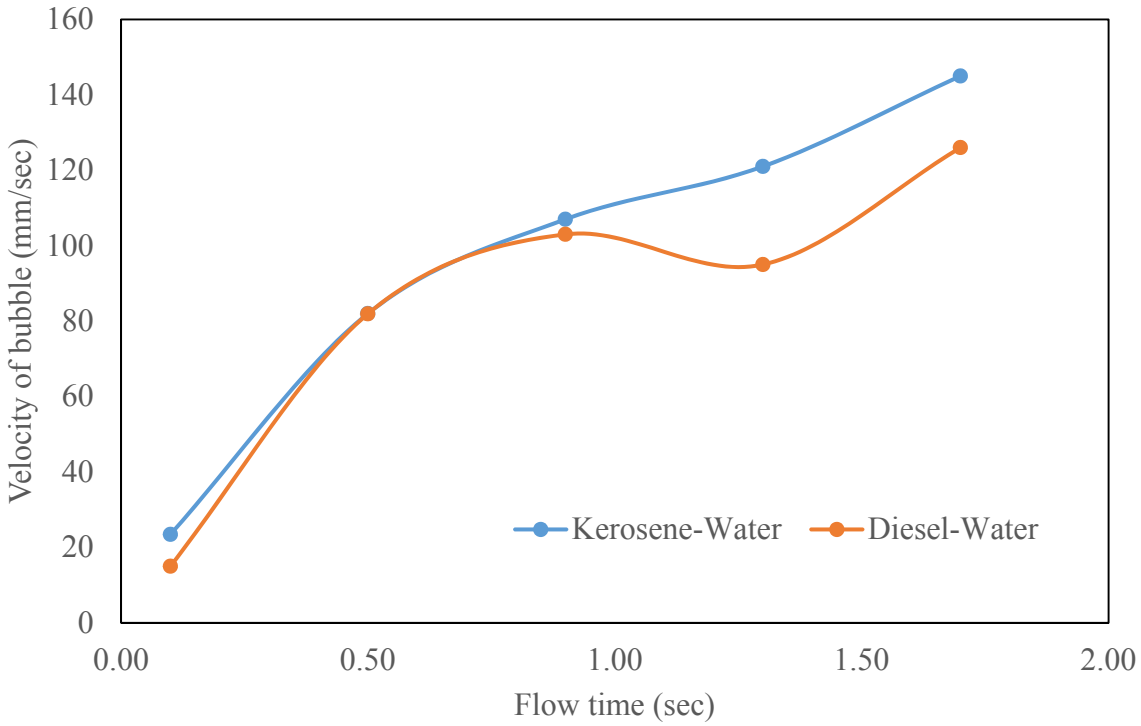

Figure 4.17: Velocity variation of air bubble with flow time for two different fluid pairs

CHAPTER 5: CONCLUSION & SCOPE OF FUTURE WORK

5.1 CONCLUSION

In this chapter, important findings obtained through the results and extensive discussions are categorically mentioned point by point.

5.1.1 Increase in Height of Entrainment with Increase in Bubble Size: We performed numerical study and calculated the maximum height of entrainment by varying the bubble diameter for different fluid pairs. The results have been plotted in graphical forms. A common tendency observed is that the height of the entrainment increases monotonously with bubble diameter. This is irrespective of the type of fluid pair.

5.1.2 VOF Method can be Successfully Implemented: Volume of Fluid (VOF) model with Finite Volume Method (FVM) is very effective to predict the maximum height of the entrainment successfully.

5.1.3 Velocity of Air Bubble Increases with Flow Time: The velocity of air bubble increases monotonously with flow time for all the cases. This is independent of the type of fluid pair selected. But in diesel-water fluid pair it becomes momentarily constant.

5.1.4 Height of Entrainment for Diesel-Water Fluid Pair is Comparatively Less than Kerosene-Water Pair: The strength of entrainment considering two fluid pairs are compared. It is found that the height of the maximum entrainment with kerosene-water fluid pair is comparatively higher than that with diesel-water fluid pair. This may be due to the difference in viscosities, interfacial tensions, densities etc. between the two fluid pairs.

5.2 SCOPE OF FUTURE WORK

In this section the further research work that can be conducted with this problem have been discussed.

- Numerical analysis of the same problem using three dimensional geometry of the container can be conducted in near future.
- Effect of initial height of the bubble from the base of the container and effect of container size and shape on the phenomena can be evaluated.

REFERENCES:

Roy, A.K., Maiti, B., Das, P.K., 2013. Visualization of air entrainment by plunging jet, Procedia Engineering 56, 468-473.

Kulkarni, A.L., Patwardhan, A.W., 2014. CFD modelling of gas entrainment in stirred tank systems, Chemical Engineering Research and Design 92, 1227-1248.

Brouilliot, D., Lubin, P., 2013. Numerical simulations of air entrainment in a plunging jet of liquid, Journal of Fluids and Structures 43, 428-440.

Liu, D., Peng, Y., 2014. Reducing the entrainment of clay minerals in flotation using tap and saline water, Powder Technology 253, 216-222.

Greene, G.A., Chen, J.C., Conlin, M.C., 1991. Bubble induced entrainment between stratified liquid layers, International Journal of Heat and Mass Transfer 34, 149-157.

Greene, G.A., Chen, J.C., Conlin, M.C., 1988. Onset of entrainment between immiscible liquid layers due to rising gas bubbles, International Journal of Heat and Mass Transfer 31, 1309-1317.

Shahrokhi, H., Shaw, J.M., 1994. The origin of fine drops in batch gas-agitated liquid-liquid systems, Chemical Engineering Science 49, 5203-5213.

Li, H., Feng, Q., Yang, S., Ou, L., Lu, Y., 2014. The entrainment behaviour of sericite in microcrystalline graphite flotation, International Journal of Mineral Processing 127, 1-9.

Agarwal, P., Verma, N., 2014. Experimental and numerical investigation of strength of inertial entrainment, Student Paper, Department of Mechanical Engineering, NIT Rourkela.

Wang, K., Bai, B., Ma, W., 2013. A model for droplet entrainment in churn flow, Chemical Engineering Science 104, 1045-1055.

Wang, K., Bai, B., Ma, W., 2013. Huge wave and drop entrainment mechanism in gas-liquid churn flow, Chemical Engineering Science 104, 638-646.

Cristofano, L., Nobili, M., Caruso, G., 2014. Experimental study on unstable free surface vortices and gas entrainment onset conditions, Experimental Thermal and Fluid Science 52, 221-229.

Verma, N., Agarwal, P., Ghosh, S., Das, A.K., 2013. Determination of strength in inertial entrainment: an experimental study, International Conference on Multiphase Flow.

Tan, S.M., Ng, H.K, Gan, S., 2013. CFD modelling of soot entrainment via thermophoretic deposition and crevice flow in a diesel engine, Journal of Aerosol Science 66, 83-95.

Tian, X.S., Zhao, H., Liu, H.F., Li, W.F., Xu, J.L, 2014. Liquid entrainment behaviour at the nozzle exit in coaxial gas-liquid jets, Chemical Engineering Science 107, 93-101.

Oka, Y., Yamaguchi, J., Muraoka, K., 2014. Decrease of carbon dioxide concentration and entrainment of horizontally spreading ceiling jet, Fire Safety Journal 63, 37-42.

Meng, Z., Wang, L., Tian, W., Qiu, S., Su, G., 2014. Entrainment at T-junction: A review work, Progress in Nuclear Energy 70, 221-241.